

1 **Assimilating summer sea-ice thickness observations**
2 **improves Arctic sea-ice forecast**

3 **Ruizhe Song^{1,2,3,4}, Longjiang Mu², Svetlana N. Loza^{3,5}, Frank Kauker³,**
4 **Xianyao Chen^{1,2}**

5 ¹Frontier Science Center for Deep Ocean Multispheres and Earth System and Physical Oceanography
6 Laboratory, Ocean University of China, Qingdao, China

7 ²Laoshan Laboratory, Qingdao, China

8 ³Alfred Wegener Institute, Helmholtz Centre for Polar and Marine Research, Bremerhaven, Germany

9 ⁴Academy of the Future Ocean, Ocean University of China, Qingdao, China

10 ⁵Shirshov Institute of Oceanology, Russian Academy of Sciences, Moscow, Russia

11 **Key Points:**

- 12 • Assimilating summer CryoSat-2 sea-ice thickness (SIT) observations makes more
13 skillful Arctic ice-edge forecasts on multiple time scales.
14 • The long-term SIT forecasts improve with the assimilation of summer CryoSat-
15 2 SIT observations.
16 • Further refinement is needed for summer CryoSat-2 SIT observations.

Corresponding author: Longjiang Mu, ljmu@qnlm.ac

Abstract

Proper Arctic sea-ice forecasting for the melt season is still a major challenge because of the recent lack of reliable pan-Arctic summer sea-ice thickness (SIT) data. A new summer CryoSat-2 SIT observation data set based on an artificial intelligence algorithm may alleviate this situation. We assess the impact of this new data set on the initialization of sea-ice forecasts in the melt seasons of 2015 and 2016 in a coupled sea ice-ocean model with data assimilation. We find that the assimilation of the summer CryoSat-2 SIT observations can reduce the summer ice-edge forecast error. Further, adding SIT observations to an established forecast system with sea-ice concentration assimilation leads to more realistic short-term summer ice-edge forecasts in the Arctic Pacific sector. The long-term Arctic-wide SIT prediction is also improved. In spite of remaining uncertainties, summer CryoSat-2 SIT observations have the potential to improve Arctic sea-ice forecast on multiple time scales.

Plain Language Summary

Arctic sea ice is rapidly declining due to global warming, especially in summer. Accurate sea-ice forecasting is important to understand the potential influence of these changes and devise effective responses. The performance of sea-ice forecasts highly depends on the accuracy of the initial sea-ice states. So refining the initial conditions of sea-ice forecasts with satellite observations is a common way to reduce forecast errors. However, obtaining reliable summer pan-Arctic satellite sea-ice thickness (SIT) data is challenging due to complex ice-surface conditions in summer. A new artificial-intelligence-based summer SIT satellite data product may mitigate this situation. We integrate this data set into a sea-ice forecast system to evaluate its impact on forecast accuracy. We find that the new summer satellite SIT data can reduce short-term ice-edge location forecast errors and benefit long-term SIT forecasts.

1 Introduction

Arctic sea ice is declining at unprecedented speed (Rothrock et al., 1999; Comiso et al., 2008; Kwok & Rothrock, 2009; Stroeve et al., 2012), which would pose challenges to climatic and ecological stakeholders (Landrum & Holland, 2020). The Arctic Passage, opening up with the gradually melting summer sea ice, calls for accurate Arctic sea-ice prediction from daily to seasonal scales (Jung et al., 2016).

Accurate initialization of sea-ice state is vital for predicting Arctic sea ice (e.g., Blanchard-Wrigglesworth et al., 2011; Guemas et al., 2016; Xie et al., 2016; Dirkson et al., 2017; Bushuk et al., 2022). The assimilation of sea-ice concentration (SIC) has improved the short-term sea-ice forecasts greatly as documented in the literature, and is now widely used at forecasting centers (e.g., Hebert et al., 2015; Lemieux et al., 2015). Sea-ice thickness (SIT) persists longer, therefore assimilation of SIT raises long-term sea-ice forecast skills even stronger (Day, Hawkins, & Tietsche, 2014; Shu et al., 2021; Mu et al., 2022).

However, the potential impacts of summer SIT observations on sea-ice forecasts are not examined comprehensively yet due to a lack of data. An effective retrieval method for the remotely sensed SIT from May to September was missing (Laxon et al., 2013; Ricker et al., 2014). The complex summer ice-surface conditions restrict the application of classical algorithms designed for winter conditions. For instance, melt ponds which occupy a huge fraction of the sea-ice surface in the melt seasons (Maykut et al., 1992) complicate the classification algorithms (Lee et al., 2018; Tilling et al., 2019) and introduce large uncertainties due to increased moisture in the snow (Drinkwater, 1991). On the other hand, in-situ Arctic SIT observations are rather scarce and localized. They can hardly be used in basin-scale assimilation systems.

64 In a recent study, Dawson et al. (2022) presented the first estimate of pan-Arctic summer
 65 sea-ice freeboard from radar altimeter by using a 1D convolutional neural network (CNN)
 66 to distinguish ice leads from melt ponds. Landy et al. (2022) converted summer CryoSat-2
 67 radar freeboard to SIT and applied further corrections. The spring predictability barrier of
 68 the Arctic sea ice (e.g., Day, Tietsche, & Hawkins, 2014; Bushuk et al., 2017) suggests that
 69 sea-ice forecast should benefit from the initialization with SIT in the melt season (Bushuk et
 70 al., 2020). Therefore, it presents an opportunity to explore the extent to which the summer
 71 SIT observation could improve the real-time forecast skill. Min et al. (2023) demonstrated
 72 that assimilation of summer SIT corrects the overestimation in the Combined Model and
 73 Satellite Thickness (CMST; Mu et al., 2018b) product. Y.-F. Zhang et al. (2023) found
 74 that the assimilation of May to August CryoSat-2 SIT anomalies improves local SIC and
 75 sea-ice extent (SIE) forecasts in September. However, the influence of assimilating summer
 76 CryoSat-2 SIT observations on short-term sea-ice forecast in summer and on long-term
 77 forecast extending beyond September still needs to be investigated further.

78 In this study, we focus on the impact of summer SIT observations on the daily and
 79 seasonal forecast skills of a sea-ice prediction modelling system. In particular, we perform
 80 a series of short- and long-term ensemble sea-ice forecasts where the sea ice-ocean initial
 81 state is constrained by the summer CryoSat-2 SIT or where these data are not used. The
 82 benefits and challenges of using these new SIT data are evaluated and critically discussed
 83 using independent sea-ice data.

84 **2 Data and Methods**

85 **2.1 The coupled sea ice-ocean model**

86 We use a regional coupled sea ice-ocean model driven by atmospheric forecasts to con-
 87 figure the sea ice-ocean forecast system. The model is based on the Massachusetts Institute
 88 of Technology general circulation model (MITgcm; Marshall et al., 1997) and covers the
 89 pan-Arctic region with a horizontal resolution of around 18 km as in Losch et al. (2010).
 90 The sea-ice model uses a viscous-plastic rheology (Hibler III, 1979; J. Zhang & Hibler III,
 91 1997) and a so called zero-layer thermodynamic formulation without heat capacity (Semtner,
 92 1976; Parkinson & Washington, 1979). The readers are referred to Losch et al. (2010) and
 93 Nguyen et al. (2011) for more details on the model.

94 **2.2 Data assimilation and forecast**

95 The summer data assimilation system is initialized from restart files generated by CMST
 96 (Mu et al., 2018b) simulation with 11 ensemble members. CMST combines model physics
 97 with information from remote-sensed SIT and SIC observations. It successfully reproduces
 98 the spatio-temporal sea-ice variations (Mu et al., 2018b). The summer data assimilation
 99 and forecast strategy follows Mu et al. (2017) and Mu et al. (2019). A Local Error Subspace
 100 Transform Kalman Filter (Nerger et al., 2012) coded within the Parallel Data Assimilation
 101 Framework (Nerger et al., 2005) is used to assimilate the summer SIT and SIC observations
 102 separately or simultaneously. Then, the summer ensemble forecasts start from the new
 103 individual analyses and the model is integrated forced by the atmospheric forecasts (cf.
 104 Section 2.3).

105 The CryoSat-2 summer SIT data set is derived from local variations in the CryoSat-2
 106 radar echo response using a deep learning method (Dawson et al., 2022; Landy et al., 2022).
 107 This is the first estimate of pan-Arctic summer SIT from satellite observations. However,
 108 the accuracy of the CryoSat-2 summer SIT still needs to be further improved after the
 109 correction introduced by Landy et al. (2022), for example over the regions north of the
 110 Greenland and the Canadian Arctic Archipelago (CAA). The summer SIT is assimilated
 111 into the system on a daily basis using the observations linearly interpolated between two
 112 biweekly records. Considering the shortcomings of the summer SIT over thick ice regions,

practical experience suggests that the observation uncertainties should be set higher than the original values over thick ice regions, while still using the provided errors over thin ice regions (Supporting Information). The SIC data used in the assimilation are computed at the French Research Institute for Exploitation of the Sea (IFREMER) based on the 85-GHz SSM/I and SSM/IS channels (Kaleschke et al., 2001; Spreen et al., 2008; Kern et al., 2010). The uncertainty of the SIC observation is set to a constant value of 0.25 following Yang, Losa, Losch, Jung, and Nerger (2015) and Yang et al. (2016).

The short-term ensemble assimilation and forecast experiments are driven by the 174-hour atmospheric ensemble forecasts from the United Kingdom Met Office (UKMO) Ensemble Prediction System (EPS; Bowler et al., 2008). For the long-term prediction, the ensemble members are driven by deterministic atmospheric forcing (single member). The hourly European Centre for Medium-Range Weather Forecasts Reanalysis v5 (ERA-5; Hersbach et al., 2020) is used as the atmospheric forcing during the data assimilation, while the atmospheric forecasts from the National Center for Environmental Prediction Climate Forecast System Version 2 (CFSv2; Saha et al., 2014) are used for the 9-month long-term forecasts.

2.3 Experiment design

In order to investigate the potential impact of the CryoSat-2 summer SIT on sea-ice forecasts, this study designs both short-term (7 days) and long-term (270 days) forecasts (Table. 1). These experiments are conducted over different months. The short-term experiments in 2015, which cover the melt season, start from the CMST restart files on May 1, May 31, June 30, July 30, and August 29, respectively. Each forecast experiment lasts for 30 days and on each day a 7-day sea-ice forecast is run using the atmospheric forcing from the daily UKMO ensemble forecasts. No data assimilation is applied in the control run of the short-term forecasts (Short-CTRL). The Short-SIT experiments assimilate only the CryoSat-2 summer SIT data, and the Short-SIC experiments assimilate only the SSMI/SSMIS SIC data, while both data sets are assimilated in the Short-SICSIT experiments. For the 2016 experiments, only the start dates are changed to match the available restart files from CMST (Table. 1).

The long-term forecast experiments are designed to diagnose the persistence of the assimilated CryoSat-2 summer SIT over the months from the melt season to the freezing season. The Long-SIT experiments with SIT assimilation start each summer month from CMST restart files and a daily data assimilation step iterating over 15 days is performed to mitigate abrupt SIT changes. Over that period, ERA5 atmospheric reanalysis forcing is used. Then, the 270-day sea-ice forecasts start from the sea-ice analysis restart files and are forced by the CFSv2 operational atmospheric forecasts. No data assimilation is performed in the Long-CTRL experiments. The forecast start dates are listed in Table 1.

2.4 Verification

Simulation output from the Pan-Arctic Ice-Ocean Modeling and Assimilation System (PIOMAS; J. Zhang & Rothrock, 2003) is employed for the comparison with the assimilation results. PIOMAS is constrained by SIC and sea surface temperature observations. Its modeled SIT has been validated to be comparable to in-situ observations and has been widely used in previous studies.

The integrated ice-edge error (IIEE; Goessling et al., 2016) is used to quantify the skill of the short-term ice-edge forecasts. It measures the discrepancy between the forecasted and observed SIE. The reference observation used in this study is the NOAA/NSIDC Climate Data Record (CDR) of Passive Microwave Sea Ice Concentration Version 4 (Meier et al., 2021).

To validate the skill of the long-term sea-ice forecast, we compute the IIEE and the RMSD of SIT against various other products and in-situ observations. The IIEE is com-

Table 1. Summary of forecast experiments design. Short: short-term forecast. Long: long-term forecast.

Experiment	Assimilated data	Forecast duration (days)	Atmospheric forcing during assimilation	Atmospheric forcing during forecast	Forecast start date
Short-CTRL	/	7	UKMO (11)	UKMO (11)	Daily forecast starting from
Short-SIT	CryoSat-2 SIT	7	UKMO (11)	UKMO (11)	05/01/2015,
Short-SIC	SSMI/SSMIS SIC	7	UKMO (11)	UKMO (11)	05/31/2015,
Short-SICSIT	SSMI/SSMIS SIC and CryoSat-2 SIT	7	UKMO (11)	UKMO (11)	06/30/2015,
Long-CTRL	/	270	ERA5 (1)	CFSv2 (1)	07/30/2015,
Long-SIT	CryoSat-2 SIT	270	ERA5 (1)	CFSv2 (1)	08/29/2015,
					04/25/2016,
					05/25/2016,
					06/24/2016,
					07/24/2016,
					08/23/2016.
					05/16/2015,
					06/15/2015,
					07/15/2015,
					08/14/2015,
					09/13/2015,
					05/10/2016,
					06/09/2016,
					07/09/2016,
					08/08/2016,
					09/07/2016.

puted using the NOAA/NSIDC SIC CDR data. The RMSDs of SIT are computed with respect to the CS2SMOS products (Ricker et al., 2017). The SIT observations derived from ULS moorings maintained by the Beaufort Gyre Exploration Program (BGEP) are used for the forecast evaluation. The three moorings BGEP-A, BGEP-B, and BGEP-D, which provide year-round sea-ice draft observations, are located at (75.0°N, 150.0°W), (78.0°N, 150.0°W) and (74.0°N, 140.0°W), respectively (Figure S1). The draft is converted to SIT by multiplying it by a constant factor of 1.1 as in Nguyen et al. (2011).

3 Result

3.1 Short-term ice-edge forecast

An overview of the SIT states of PIOMAS, CryoSat-2, and the short-term experiment assimilation results in 2015 is shown in Figure 1 and in 2016 in Figure S2. In May and June, CryoSat-2 has similar SIT over the compact ice regions but thinner (by more than 0.5 m) ice over the first-year ice regions compared to the PIOMAS SIT. This is more evident in July, August, and September, while the CryoSat-2 SIT is biased low over the central Arctic. Landy et al. (2022) pointed out that the roughness-induced electromagnetic range bias on the heavily-deformed ice in the coast regions north of the CAA and Greenland are responsible for these underestimates. In general, the SIT patterns of CryoSat-2 observations are more similar to the Short-CTRL patterns, which are the extensions of CMST, than to the PIOMAS patterns. Short-CTRL SIT patterns have thinner ice in the Beaufort Sea than the PIOMAS patterns, capturing an expected SIT distribution. This is not surprising since CMST is constructed by assimilating remote-sensed SIT during the freezing season until April (Mu et al., 2018b), while PIOMAS does not assimilate any SIT (J. Zhang & Rothrock, 2003).

The area-averaged SIT differences between Short-SIT and Short-CTRL in May to September of 2015 are 0.10 m, -0.06 m, -0.37 m, -0.37 m and -0.39 m, respectively. Overall, the area-averaged SIT differences are smallest in May and June, when the assimilation of the summer CryoSat-2 observations reduces the SIT in the Amerasian Basin and increases it in the Eurasian Basin. In the strong melt months of July, August and September, when the uncertainties of the CryoSat-2 SIT are at their maximum, the underestimation of the SIT over the multi-year ice regions, i.e., north of the CAA and Greenland, is remarkable. The differences can easily exceed -1 m and even reach -1.5 m. SIT is also reduced in most of the marginal ice zones, especially in the Beaufort Sea and the Chukchi Sea. CMST tends to overestimate late summer SIT in the marginal seas due to unrealistic covariances between SIC and SIT when abrupt increases in SIC are triggered by wind convergences (Mu et al., 2018b). The assimilation of CryoSat-2 SIT corrects this bias, resulting in a more reasonable estimate of SIT in the marginal seas.

SIT assimilation has an important impact on SIC simulations through the physical connection between thickness and concentration (Xie et al., 2016; Mignac et al., 2022). Short-term forecast of ice edge, defined as the 15% SIC isoline, can be strongly influenced by SIT assimilation. Figure 2 shows the reduction of IIEE in the Pacific sector and Atlantic sector (regions shown in Figure S1). IIEE in each forecast experiment is given in Figure S3. The observed SIC used as the reference for the IIEE calculation is the NOAA/NSIDC SIC CDR. The difference in the ice-edge position between forecasts and observations in 2015 and 2016 is displayed in Figure S4 and Figure S5.

The impact of CryoSat-2 SIT assimilation on ice-edge forecasts varies with time and region. Compared to Short-CTRL, IIEE in Short-SIT is strongly reduced in most times and both sectors (Figure 2). In the Pacific sector, the ice-edge position in the forecasts is consistently overestimated in Short-CTRL. Assimilation of the summer SIT reduces the SIT of the forecasts near the ice edge, resulting in a better agreement between the ice-edge forecasts and the ice-edge observations from the satellite (Figure S4 and Figure S5).

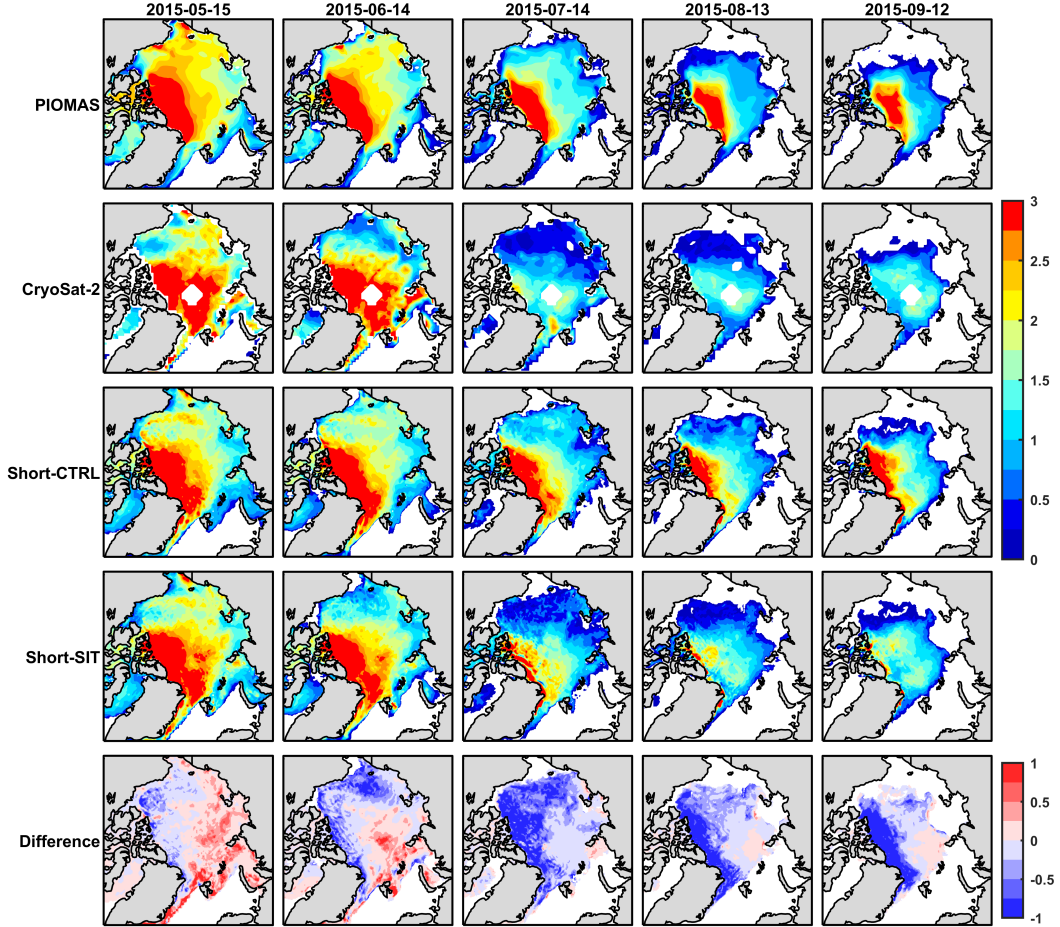


Figure 1. SIT (m) in PIOMAS, CryoSat-2, Short-CTRL, Short-SIT, and the difference between Short-SIT and Short-CTRL 15 days after the start in May to September of 2015. Note that CryoSat-2 observations are two-week averages while the rest are daily SIT.

212 In May and June, only a slight improvement in IIEE is observed. However, in July,
 213 especially in 2015, IIEE increases. This can be attributed to the fact that the melt-pond
 214 fraction starts to increase in June and reaches its maximum in July (Feng et al., 2022).
 215 In particular, the melt-pond fraction in the Beaufort Sea peaked in 2015 during the 2000-
 216 2021 observation period (Xiong & Ren, 2023). The presence of excessive melt-pond fraction
 217 may lead to more misclassification of ice leads and melt ponds in the CryoSat-2 sea-ice
 218 freeboard retrieval using the CNN model, which affects the SIT analysis in the Pacific
 219 sector. Therefore, the underestimated SIT erroneously leads to a large ice-edge error in July
 220 of the Short-SIT experiments. This warrants further refinement of the artificial intelligence
 221 algorithm used for summer CryoSat-2 SIT retrieval. In late summer, the assimilation of
 222 CryoSat-2 SIT observations in Short-SIT leads to more skillful ice-edge forecasts, resulting
 223 in a statistically significant average reduction in IIEE of about $2.1 \times 10^5 \text{ km}^2$. For example,
 224 the assimilation of SIT allows the model to predict an ice-free "cave" inside the Beaufort
 225 Sea in August 2015, while it is completely covered by sea ice in Short-CTRL (Figure S4).
 226 Furthermore, the ice-edge forecasts in the Atlantic sector are also improved, especially in
 227 June (about $0.8 \times 10^5 \text{ km}^2$) and July (more than $0.9 \times 10^5 \text{ km}^2$).

We further investigate the influences of SIC assimilation together with summer SIT assimilation on the ice-edge forecasts, considering the more important role of SIC observations on summer sea-ice forecasts as documented in the literature (e.g., Posey et al., 2015; Yang, Losa, Losch, Liu, et al., 2015). Forecasts from the Short-SICSIT experiments are also compared to the Short-SIC experiments, which performs SIC assimilation only.

In the Pacific sector, the additional SIT assimilation tends to yield more favorable ice-edge forecasts compared to Short-SIC (Figure 2). Similar to the IIEE differences between Short-SIT and Short-CTRL, the improvement in May and June between Short-SICSIT and Short-SIC is relatively small (only 3.0×10^3 km² on average). In July, IIEE becomes smaller in 2015 but larger in 2016 relative to Short-SIC. In late summer, the analysis of summer SIT observations significantly reduces the IIEE, bringing the ice-edge forecasts closer to the observations. In the Atlantic Sector, Short-SICSIT does not yield overwhelmingly better results than Short-SIC (Figure 2). The introduction of summer CryoSat-2 SIT observations gives rise to larger IIEE in May and June, while the IIEE differences are smaller in later months. Nevertheless, these mean IIEE differences are still in the range of $\pm 0.5 \times 10^5$ km², which is much smaller than the changes between Short-SIT and Short-CTRL. In the Atlantic sector Short-SIC is already close to the observations due to a reasonable CMST SIT estimate north of the Svalbard and Novaya Zemlya, so further improvements are rather limited.

Note that, as shown by the solid lines representing the mean IIEE differences in Figure 2, the effect of the summer CryoSat-2 SIT assimilation is gradually more evident in most of the months in the Short-SICSIT experiments. The improvements of Short-SICSIT relative to Short-SIC become larger with increasing lead time, while the deteriorations of IIEE become smaller, with the exception of the June 2016 forecasts.

3.2 Long-term sea-ice forecast

The Long-SIT experiments with summer CryoSat-2 SIT assimilation provides significant benefits for ice-edge and thickness forecasts, as shown in Figure 3. Reductions in IIEEs are found in May, June and August in 2015 and in 2016 for the first 30 days (Figure 3a, b). In July, the CryoSat-2 SIT assimilation is only effective for a few days due to the underestimated thickness uncertainties caused by melt ponds. The improvement in ice-edge forecast is also pronounced in September, for three weeks in 2015 and two weeks in 2016: As freezing begins, the IIEE difference gradually increases.

With respect to the CS2SMOS SIT product, the predicted Arctic-wide thickness is also improved (Figure 3c, d), except for the forecast starting in July 2016, which degrades after 140 days. The summer CryoSat-2 SIT mitigates the SIT overestimation in the Beaufort Sea in Long-CTRL that is initialized from the CMST state (not shown). The improvements are most pronounced in October, when the freezing season begins, and decrease exponentially with time until the forecast system falls into the control of the internal variability. This superior skill may even persist throughout the freezing season, similar to the previous findings on an optimal winter SIT initialization improving the predictive skill of summer sea ice (Blockley & Peterson, 2018). Consistent with the performance of the short-term forecasts in section 3.1, the reduction of SIT RMSD in 2015 is more significant than that in 2016, because relatively small SIT difference between summer CryoSat-2 observations and the CMST estimate is observed in 2016.

We also examine the performance of the long-term SIT forecasts at the BGEP sites (Figure S6). In general, significant improvements in the SIT forecasts are found in Long-SIT initialized in July, August and September of 2015. The differences between Long-SIT and Long-CTRL in 2016 are limited, not exceeding 30 cm most of the time. The forecasts tend to overestimate SIT in the early freezing season in the Beaufort Sea. To check if the reason is within the biases of long-term atmospheric forecasts, we performed additional forecast experiments in 2015 (not shown) with the same configuration as Long-CTRL, except that the CFSv2 atmospheric forecast is replaced by the ERA-5 reanalysis for the atmospheric

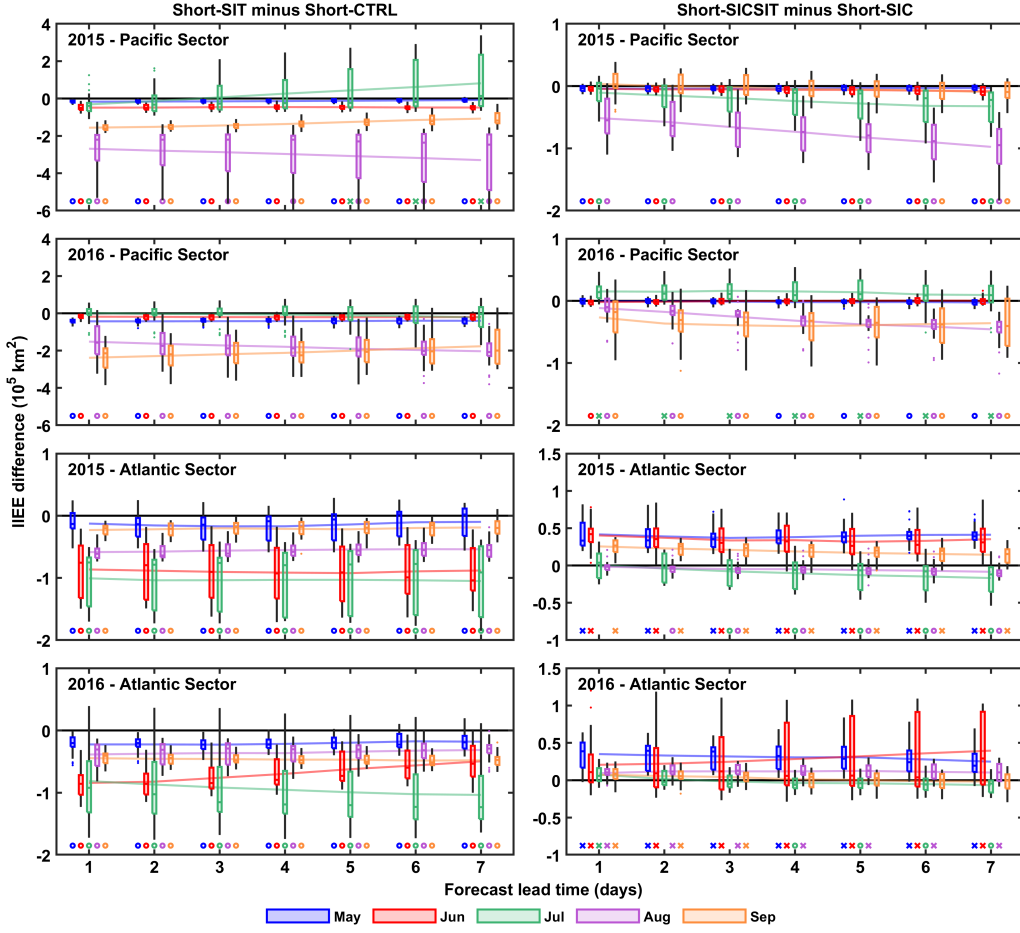


Figure 2. Box plot of the IIEE difference ($10^5 km^2$) between Short-SIT and Short-CTRL (left), together with that between Short-SICSIT and Short-SIC (right) in the 7-day sea-ice forecasts. The IIEE in the box plot is calculated after 7 days of assimilation when the summer CryoSat-2 SIT is fully effective. Blue, red, green, purple and orange boxes indicate different summer months. Colored boxes indicate IIEE difference between the lower and upper quartiles. Colored outliers denote values more than 1.5 interquartile range from the top or bottom of the colored box. The outer edges of the black lines denote the minimum and maximum values that are not outliers. Solid-colored lines show the mean IIEE difference at each lead time. A positive value indicates an increase in IIEE, when SIT is assimilated, while a negative value indicates a decrease in the IIEE. Markers at the bottom of each panel indicate increases (cross) and decreases (circle) in IIEE that pass the Student’s T-test at the 95% confidence level. Note that negative values indicate better forecast skills.

279 forcing. The ERA-5 driven simulations show a similar overestimation of SIT in the Beaufort
 280 Sea. The anticyclonic wind in the Beaufort Gyre pushes excessively thick ice from the multi-
 281 year ice region north of the CAA into the Beaufort Sea as in Long-CTRL. This suggests
 282 that the overestimation is not mainly due to biases in the atmospheric forcing but imperfect
 283 model parameterizations and initial ice-ocean conditions.

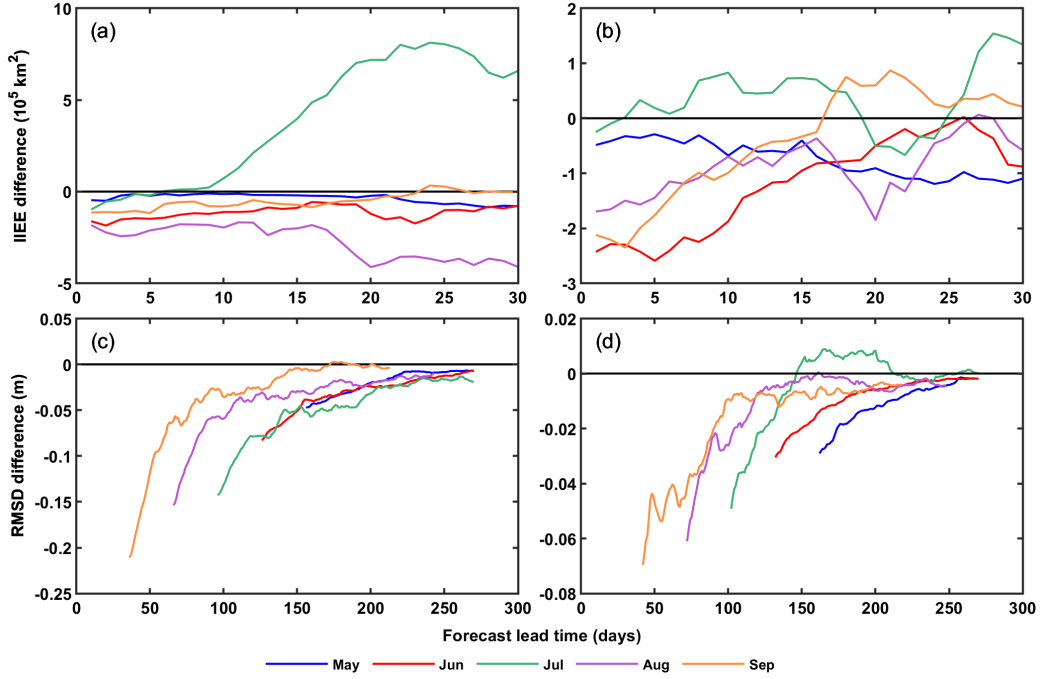


Figure 3. The difference of the IIEE ($10^5 km^2$) in 2015 (a) and in 2016 (b), and the difference of the RMSD of the SIT (m) in 2015 (c) and in 2016 (d) between the Long-SIT and Long-CTRL forecasts initialized from May to September. The RMSD of the SIT is computed with respect to the CS2SMOS product available from October to April, hence the staggered time series in (c) and (d). Note that negative values indicate better forecast skill.

284 **4 Summary**

285 This study examines the impact of summer CryoSat-2 SIT assimilation on short- and
 286 long-term sea-ice forecasts in 2015 and in 2016. The ice-edge forecasts with summer CryoSat-2
 287 SIT assimilation are dramatically improved when compared to the experiments without
 288 any data assimilation. When the summer CryoSat-2 SIT data are assimilated together with
 289 SIC data, the effects on the ice-edge forecast skill are rather dependent on the time when the
 290 forecast is initialized and are spatially highly variable. In the Pacific sector, the combined
 291 assimilation of summer SIT and SIC observations leads to more realistic summer ice-edge
 292 forecasts with a one-week lead time.

293 The long-term sea-ice forecasts show significant reductions in both IIEE and RMSD
 294 of the SIT, except for those initialized in July, when the summer CryoSat-2 SIT has large
 295 uncertainties. The improvement in ice-edge forecasts can last up to about 30 days, while for
 296 the SIT forecasts the benefits can last for more than 3 months. This result demonstrates
 297 that, although the atmospheric forecasts used to drive the model can evolve freely after
 298 about one month, the SIT initialization in summer remains a primary factor in predicting
 299 long-term SIT variations.

300 However, limitations of the summer CryoSat-2 SIT data product still remain. The deep
 301 learning algorithm used has a certain degree of uncertainty in classifying ice leads and melt
 302 ponds, especially when the melt-pond fraction is large. The underestimation in the sum-
 303 mer CryoSat-2 SIT from July to September in the coastal regions north of the CAA and
 304 Greenland requires further work on the sea-ice freeboard and thickness retrieval algorithm

305 or exploration of new correction schemes to improve their reliability and accuracy. Further-
 306 more, it is still an open question how this product should be used for real-time Arctic sea-ice
 307 forecasting, since its uncertainty currently does not account for all the algorithm errors, and
 308 possible representation errors (Janjić et al., 2018) should be considered accurately.

309 5 Open Research

310 The ensemble mean Arctic sea-ice thickness (SIT) and sea-ice concentration (SIC) fore-
 311 cast data used in the study can be downloaded at Song et al. (2024). The file size of the
 312 forecast results with all ensemble members exceeds 50GB and can be made available upon re-
 313 quest through contact. The CMST SIT estimate is available at Mu et al. (2018a). The sum-
 314 mer CryoSat-2 SIT observations can be downloaded from Landy and Dawson (2022). The
 315 SSMI/SSMIS SIC data is available from Kern et al. (2024). The UKMO atmospheric ense-
 316 mble forecasts are available in the THORPEX Interactive Grand Global Ensemble (TIGGE;
 317 Bougeault et al., 2010) archive (<https://apps.ecmwf.int/datasets/data/tigge>). The
 318 hourly ERA5 reanalysis is available at Hersbach et al. (2023). The CFSv2 atmospheric fore-
 319 casts are available at [https://www.ncei.noaa.gov/products/weather-climate-models/
 320 climate-forecast-system](https://www.ncei.noaa.gov/products/weather-climate-models/climate-forecast-system). The PIOMAS (J. Zhang & Rothrock, 2003) data is provided
 321 at <https://psc.apl.uw.edu/data>. The NOAA/NSIDC SIC CDR data is available at
 322 Meier et al. (2021). The CS2SMOS data is available at <https://www.meereisportal.de>.
 323 Mooring observations from BGEF are downloaded from [https://www2.whoi.edu/site/
 324 beaufortgyre](https://www2.whoi.edu/site/beaufortgyre).

325 Acknowledgments

326 This study is supported by the National Key R&D Program of China under Grant 2019YFA0607000,
 327 the National Natural Science Foundation of China (42176235) and the Laoshan Laboratory
 328 (LSKJ202202300). Contribution of SNL was supported by the Federal Ministry of Educa-
 329 tion and Research of Germany in the framework of the Seamless Sea Ice Prediction project
 330 (SSIP, Grant 01LN1701A) and partly made in the framework of the state assignment of
 331 SIO RAS (theme FMWE-2024-0028).

332 References

- 333 Blanchard-Wrigglesworth, E., Bitz, C. M., & Holland, M. M. (2011, 09). Influence of initial
 334 conditions and climate forcing on predicting arctic sea ice. *Geophysical Research
 335 Letters*, *38*, L18503. doi: 10.1029/2011GL048807
- 336 Blockley, E. W., & Peterson, K. A. (2018). Improving met office seasonal predictions
 337 of arctic sea ice using assimilation of cryosat-2 thickness. *The Cryosphere*, *12*(11),
 338 3419-3438. doi: 10.5194/tc-12-3419-2018
- 339 Bougeault, P., Toth, Z., Bishop, C., Brown, B., Burridge, D., Chen, D. H., ... Worley, S.
 340 (2010). The thorpeX interactive grand global ensemble. *Bulletin of the American
 341 Meteorological Society*, *91*(8), 1059-1072. doi: 10.1175/2010BAMS2853.1
- 342 Bowler, N. E., Arribas, A., Mylne, K. R., Robertson, K. B., & Beare, S. E. (2008). The
 343 mogreps short-range ensemble prediction system. *Quarterly Journal of the Royal
 344 Meteorological Society*, *134*(632), 703-722. doi: 10.1002/qj.234
- 345 Bushuk, M., Msadek, R., Winton, M., Vecchi, G. A., Gudgel, R., Rosati, A., & Yang, X.
 346 (2017). Skillful regional prediction of arctic sea ice on seasonal timescales. *Geophysical
 347 Research Letters*, *44*(10), 4953-4964. doi: 10.1002/2017GL073155
- 348 Bushuk, M., Winton, M., Bonan, D. B., Blanchard-Wrigglesworth, E., & Delworth, T. L.
 349 (2020). A mechanism for the arctic sea ice spring predictability barrier. *Geophysical
 350 Research Letters*, *47*(13), e2020GL088335. doi: 10.1029/2020GL088335
- 351 Bushuk, M., Zhang, Y., Winton, M., Hurlin, B., Delworth, T., Lu, F., ... Zeng, F. (2022,
 352 07). Mechanisms of regional arctic sea ice predictability in two dynamical seasonal
 353 forecast systems. *Journal of Climate*, *35*, 4207-4231. doi: 10.1175/JCLI-D-21-0544.1

- 354 Comiso, J. C., Parkinson, C. L., Gersten, R., & Stock, L. (2008). Accelerated decline in
355 the arctic sea ice cover. *Geophysical Research Letters*, *35*(1), L01703. doi: 10.1029/
356 2007GL031972
- 357 Dawson, G., Landy, J., Tsamados, D. M., Komarov, A. S., Howell, S., Heorton, H., &
358 Krumpfen, T. (2022, 01). A 10-year record of arctic summer sea ice freeboard from
359 cryosat-2. *Remote Sensing of Environment*, *268*, 112744. doi: 10.1016/j.rse.2021
360 .112744
- 361 Day, J. J., Hawkins, E., & Tietsche, S. (2014). Will arctic sea ice thickness initialization
362 improve seasonal forecast skill? *Geophysical Research Letters*, *41*, 7566-7575. doi:
363 10.1002/2014GL061694
- 364 Day, J. J., Tietsche, S., & Hawkins, E. (2014). Pan-arctic and regional sea ice predictability:
365 initialization month dependence. *Journal of Climate*, *27*(12), 4371-4390. doi: 10.1175/
366 JCLI-D-13-00614.1
- 367 Dirkson, A., Merryfield, W. J., & Monahan, A. H. (2017). Impacts of sea ice thickness
368 initialization on seasonal arctic sea ice predictions. *Journal of Climate*, *30*, 1001-1017.
369 doi: 10.1175/JCLI-D-16-0437.1
- 370 Drinkwater, M. R. (1991). K_u band airborne radar altimeter observations of marginal sea
371 ice during the 1984 marginal ice zone experiment. *Journal of Geophysical Research:
372 Oceans*, *96*(C3), 4555-4572. doi: 10.1029/90JC01954
- 373 Feng, J., Zhang, Y., Cheng, Q., & Tsou, J. Y. (2022). Pan-arctic melt pond fraction trend,
374 variability, and contribution to sea ice changes. *Global and Planetary Change*, *217*,
375 103932. doi: 10.1016/j.gloplacha.2022.103932
- 376 Goessling, H. F., Tietsche, S., Day, J. J., Hawkins, E., & Jung, T. (2016). Predictability
377 of the arctic sea-ice edge. *Geophysical Research Letters*, *43*, 1642-1650. doi: 10.1002/
378 2015GL067232
- 379 Guemas, V., Blanchard-Wrigglesworth, E., Chevallier, M., Day, J. J., Déqué, M., Doblas-
380 Reyes, F. J., ... Tietsche, S. (2016). A review on arctic sea ice predictability and
381 prediction on seasonal-to-decadal timescales. *Quarterly Journal of the Royal Meteorological
382 Society*, *142*, 546-561. doi: 10.1002/qj.2401
- 383 Hebert, D. A., Allard, R. A., Metzger, E. J., Posey, P. G., Preller, R. H., Wallcraft, A. J.,
384 ... Smedstad, O. M. (2015, 11). Short-term sea ice forecasting: An assessment of ice
385 concentration and ice drift forecasts using the u.s. navy's arctic cap nowcast/forecast
386 system. *Journal of Geophysical Research: Oceans*, *120*, 8327-8345. doi: 10.1002/
387 2015JC011283
- 388 Hersbach, H., Bell, B., Berrisford, P., Biavati, G., Horányi, A., Muñoz Sabater, J., ... Thé-
389 paut, J.-N. (2023). *Era5 hourly data on single levels from 1940 to present* [dataset].
390 Copernicus Climate Change Service (C3S) Climate Data Store (CDS). Retrieved
391 from [https://cds.climate.copernicus.eu/cdsapp#!/dataset/reanalysis-era5-
392 -single-levels?tab=overview](https://cds.climate.copernicus.eu/cdsapp#!/dataset/reanalysis-era5-single-levels?tab=overview) doi: 10.24381/cds.adbb2d47
- 393 Hersbach, H., Bell, B., Berrisford, P., Hirahara, S., Horányi, A., Muñoz-Sabater, J., ...
394 Thépaut, J.-N. (2020). The era5 global reanalysis. *Quarterly Journal of the Royal
395 Meteorological Society*, 1999-2049. doi: 10.1002/qj.3803
- 396 Hibler III, W. D. (1979). A dynamic thermodynamic sea ice model. *Journal of Physical
397 Oceanography*, *9*, 815-846. doi: 10.1175/1520-0485(1979)009<0815:ADTSIM>2.0.CO;
398 2
- 399 Janjić, T., Bormann, N., Bocquet, M., Carton, J. A., Cohn, S. E., Dance, S. L., ... Weston,
400 P. (2018). On the representation error in data assimilation. *Quarterly Journal of the
401 Royal Meteorological Society*, *144*(713), 1257-1278. doi: 10.1002/qj.3130
- 402 Jung, T., Gordon, N. D., Bauer, P., Bromwich, D. H., Chevallier, M., Day, J. J., ... Yang,
403 Q. (2016). Advancing polar prediction capabilities on daily to seasonal time scales.
404 *Bulletin of the American Meteorological Society*, *97*, 160113112747009. doi: 10.1175/
405 BAMS-D-14-00246.1
- 406 Kaleschke, L., Lüpkes, C., Vilna, T., Haarpaintner, J., Borchert, A., Hartmann, J., &
407 Heygster, G. (2001). Ssm/i sea ice remote sensing for mesoscale ocean-atmosphere
408 interaction analysis. *Canadian Journal of Remote Sensing*, *27*, 526-537. doi: 10.1080/

- 07038992.2001.10854892
- 409 Kern, S., Kaleschke, L., Girard-Arduin, F., Spreen, G., & Beitsch, A. (2024). *Global daily*
 410 *gridded 5-day median-filtered, gap-filled asi algorithm ssmi-ssmis sea ice concentration*
 411 *data* [dataset]. Integrated Climate Data Center. Retrieved from [https://www.cen.uni-](https://www.cen.uni-hamburg.de/en/icdc/data/cryosphere/seaiceconcentration-asi-ssmi.html)
 412 [hamburg.de/en/icdc/data/cryosphere/seaiceconcentration-asi-ssmi.html](https://www.cen.uni-hamburg.de/en/icdc/data/cryosphere/seaiceconcentration-asi-ssmi.html)
 413
- 414 Kern, S., Kaleschke, L., & Spreen, G. (2010). Climatology of the nordic (irminger, greenland,
 415 barents, kara and white/pechora) seas ice cover based on 85 ghz satellite microwave
 416 radiometry: 1992–2008. *Tellus A*, *62*, 411-434. doi: 10.3402/tellusa.v62i4.15709
- 417 Kwok, R., & Rothrock, D. A. (2009). Decline in arctic sea ice thickness from submarine and
 418 icesat records: 1958-2008. *Geophysical Research Letters*, *36*, L15501. doi: 10.1029/
 419 2009GL039035
- 420 Landrum, L., & Holland, M. M. (2020, 12). Extremes become routine in an emerging new
 421 arctic. *Nature Climate Change*, *10*, 1-8. doi: 10.1038/s41558-020-0892-z
- 422 Landy, J. C., & Dawson, G. J. (2022). *Year-round arctic sea ice thickness from cryosat-*
 423 *2 baseline-d level 1b observations 2010-2020 (version 1.0)* [dataset]. NERC EDS UK
 424 Polar Data Centre. Retrieved from [https://data.bas.ac.uk/full-record.php?id=](https://data.bas.ac.uk/full-record.php?id=GB/NERC/BAS/PDC/01613)
 425 [GB/NERC/BAS/PDC/01613](https://data.bas.ac.uk/full-record.php?id=GB/NERC/BAS/PDC/01613) doi: 10.5285/d8c66670-57ad-44fc-8fef-942a46734ecb
- 426 Landy, J. C., Dawson, G. J., Tsamados, M., Bushuk, M., Stroeve, J. C., Howell, S. E. L.,
 427 ... Aksenov, Y. (2022). A year-round satellite sea-ice thickness record from cryosat-2.
 428 *Nature*, *609*, 1-6. doi: 10.1038/s41586-022-05058-5
- 429 Laxon, S. W., Giles, K. A., Ridout, A. L., Wingham, D. J., Willatt, R., Cullen, R., ...
 430 Davidson, M. (2013). Cryosat-2 estimates of arctic sea ice thickness and volume.
 431 *Geophysical Research Letters*, *40*(4), 732-737. doi: 10.1002/grl.50193
- 432 Lee, S., Kim, H.-C., & Im, J. (2018). Arctic lead detection using a waveform mixture
 433 algorithm from cryosat-2 data. *The Cryosphere*, *12*(5), 1665-1679. doi: 10.5194/
 434 tc-12-1665-2018
- 435 Lemieux, J.-F., Beaudoin, C., Dupont, F., Roy, F., Smith, G. C., Shlyaeva, A., ... Ferry, N.
 436 (2015, 03). The regional ice prediction system (rips): Verification of forecast sea ice
 437 concentration. *Quarterly Journal of the Royal Meteorological Society*, *142*, 632-643.
 438 doi: 10.1002/qj.2526
- 439 Losch, M., Menemenlis, D., Campin, J.-M., Heimbach, P., & Hill, C. (2010). On the
 440 formulation of sea-ice models. part 1: Effects of different solver implementations and
 441 parameterizations. *Ocean Modelling*, *33*(1), 129-144. doi: 10.1016/j.ocemod.2009.12
 442 .008
- 443 Marshall, J., Adcroft, A., Hill, C., Perelman, L., & Heisey, C. (1997). A finite-volume,
 444 incompressible navier stokes model for studies of the ocean on parallel computers.
 445 *Journal of Geophysical Research*, *102*, 5753-5766. doi: 10.1029/96JC02775
- 446 Maykut, G. A., Grenfell, T. C., & Weeks, W. (1992). On estimating spatial and temporal
 447 variations in the properties of ice in the polar oceans. *Journal of Marine Systems*, *3*,
 448 41-72. doi: 10.1016/0924-7963(92)90030-C
- 449 Meier, W. N., Fetterer, F., Windnagel, A. K., & Stewart, J. S. (2021). *Noaa/nsidc cli-*
 450 *mate data record of passive microwave sea ice concentration, version 4* [dataset]. Na-
 451 tional Snow and Ice Data Center. Retrieved from [https://nsidc.org/data/G02202/](https://nsidc.org/data/G02202/versions/4)
 452 [versions/4](https://nsidc.org/data/G02202/versions/4) doi: 10.7265/efmz-2t65
- 453 Mignac, D., Martin, M., Fiedler, E., Blockley, E., & Fournier, N. (2022, 02). Improving
 454 the met office’s forecast ocean assimilation model (foam) with the assimilation of
 455 satellite-derived sea-ice thickness data from cryosat-2 and smos in the arctic. *Quarterly*
 456 *Journal of the Royal Meteorological Society*, *148*, 1-24. doi: 10.1002/qj.4252
- 457 Min, C., Yang, Q., Luo, H., Chen, D., Krumpen, T., Mammun, N., ... Nerger, L. (2023).
 458 Improving arctic sea-ice thickness estimates with the assimilation of cryosat-2 summer
 459 observations. *Ocean-Land-Atmosphere Research*, *2*, 0025. doi: 10.34133/olar.0025
- 460 Mu, L., Liang, X., Yang, Q., Liu, J., & Zheng, F. (2019). Arctic ice ocean prediction system:
 461 evaluating sea ice forecasts during xuelong’s first trans-arctic passage in summer 2017.
 462 *Journal of Glaciology*, 1-9. doi: 10.1017/jog.2019.55
- 463 Mu, L., Losch, M., Yang, Q., Ricker, R., Losa, S. N., & Nerger, L. (2018a). *The arc-*

- 464 *tic combined model and satellite sea ice thickness (cmst) dataset* [dataset]. PAN-
 465 GAEA. Retrieved from <https://doi.org/10.1594/PANGAEA.891475> doi: 10.1594/
 466 PANGAEA.891475
- 467 Mu, L., Losch, M., Yang, Q., Ricker, R., Losa, S. N., & Nerger, L. (2018b). Arctic-
 468 wide sea ice thickness estimates from combining satellite remote sensing data and a
 469 dynamic ice-ocean model with data assimilation during the cryosat-2 period. *Journal*
 470 *of Geophysical Research: Oceans*, *123*, 7763-7780. doi: 10.1029/2018JC014316
- 471 Mu, L., Nerger, L., Streffing, J., Tang, Q., Niraula, B., Zampieri, L., ... Goessling,
 472 H. F. (2022). Sea-ice forecasts with an upgraded awi coupled prediction sys-
 473 tem. *Journal of Advances in Modeling Earth Systems*, *14*(12), e2022MS003176. doi:
 474 10.1029/2022MS003176
- 475 Mu, L., Yang, Q., Losch, M., Losa, S. N., Ricker, R., Nerger, L., & Liang, X. (2017). Im-
 476 proving sea ice thickness estimates by assimilating cryosat-2 and smos sea ice thickness
 477 data simultaneously: Cryosat-2 and smos sea ice thickness data assimilation. *Quarterly*
 478 *Journal of the Royal Meteorological Society*, *144*, 529-538. doi: 10.1002/qj.3225
- 479 Nerger, L., Hibler III, W. D., & SCHRÖTER, J. (2005). Pdfaf-the parallel data assimilation
 480 framework: Experiences with kalman filtering. *World Scientific*, 63-83. doi: 10.1142/
 481 9789812701831_0006
- 482 Nerger, L., Janjić, T., Schröter, J., & Hiller, W. (2012). A regulated localization scheme for
 483 ensemble-based kalman filters. *Quarterly Journal of the Royal Meteorological Society*,
 484 *138*(664), 802-812. doi: 10.1002/qj.945
- 485 Nguyen, A. T., Menemenlis, D., & Kwok, R. (2011). Arctic ice-ocean simulation with opti-
 486 mized model parameters: Approach and assessment. *Journal of Geophysical Research:*
 487 *Oceans*, *116*, C04025. doi: 10.1029/2010JC006573
- 488 Parkinson, C. L., & Washington, W. M. (1979). A large-scale numerical model of sea ice.
 489 *Journal of Geophysical Research*, *84*, 311-337. doi: 10.1029/JC084iC01p00311
- 490 Posey, P., Metzger, E., Wallcraft, A., Hebert, D., Allard, R., Smedstad, O., ... Helfrich,
 491 S. (2015, 08). Improving arctic sea ice edge forecasts by assimilating high horizontal
 492 resolution sea ice concentration data into the us navy's ice forecast systems. *The*
 493 *Cryosphere*, *9*, 1735-1745. doi: 10.5194/tc-9-1735-2015
- 494 Ricker, R., Hendricks, S., Helm, V., Skourup, H., & Davidson, M. (2014). Sensitivity of
 495 cryosat-2 arctic sea-ice freeboard and thickness on radar-waveform interpretation. *The*
 496 *Cryosphere*, *8*, 1607-1622. doi: 10.5194/tc-8-1607-2014
- 497 Ricker, R., Hendricks, S., Kaleschke, L., Tian-Kunze, X., King, J., & Haas, C. (2017). A
 498 weekly arctic sea-ice thickness data record from merged cryosat-2 and smos satellite
 499 data. *The Cryosphere*, *11*(4), 1607-1623. doi: 10.5194/tc-11-1607-2017
- 500 Rothrock, D. A., Yu, Y., & Maykut, G. A. (1999). Thinning of the arctic sea-ice cover.
 501 *Geophysical Research Letters*, *26*, 3469-3472. doi: 10.1029/1999GL010863
- 502 Saha, S., Moorthi, S., Wu, X., Wang, J., Nadiga, S., Tripp, P., ... Becker, E. (2014). The
 503 ncep climate forecast system version 2. *Journal of Climate*, *27*, 2185-2208. doi:
 504 10.1175/JCLI-D-12-00823.1
- 505 Schlitzer, R. (2023). *Ocean data view* [software]. Retrieved from <https://odv.awi.de>
- 506 Semtner, A. J. (1976). A model for thermodynamic growth of sea ice in numeri-
 507 cal investigations of climate. *Journal of Physical Oceanography*, *6*, 379-389. doi:
 508 10.1175/1520-0485(1976)006<0379:AMFTTG>2.0.CO;2
- 509 Shu, Q., Qiao, F., Liu, J., Song, Z., Chen, Z., Zhao, J., ... Song, Y. (2021). Arctic sea ice
 510 concentration and thickness data assimilation in the fio-esm climate forecast system.
 511 *Acta Oceanologica Sinica*, *40*, 65-75. doi: 10.1007/s13131-021-1768-4
- 512 Song, R., Mu, L., Kauker, F., Loza, S., & Chen, X. (2024). *Forecast data for the paper:*
 513 *"assimilating summer sea-ice thickness observations improves arctic sea-ice forecast"*
 514 [dataset]. Zenodo. Retrieved from <https://doi.org/10.5281/zenodo.10589315> doi:
 515 10.5281/zenodo.10589315
- 516 Spreen, G., Kaleschke, L., & Heygster, G. (2008). Sea ice remote sensing using amsr-e 89-ghz
 517 channels. *Journal of Geophysical Research*, *113*, C02S03. doi: 10.1029/2005JC003384
- 518 Stroeve, J. C., Serreze, M. C., Holland, M. M., Kay, J. E., Malanik, J., & Barrett, A. P.

- 519 (2012, 02). The arctic's rapidly shrinking sea ice cover: A research synthesis. *Climatic*
520 *Change*, *110*, 1005-1027. doi: 10.1007/s10584-011-0101-1
- 521 Tilling, R., Ridout, A., & Shepherd, A. (2019). Assessing the impact of lead and floe
522 sampling on arctic sea ice thickness estimates from envisat and cryosat-2. *Journal of*
523 *Geophysical Research: Oceans*, *124*, 7473–7485. doi: 10.1029/2019JC015232
- 524 Xie, J., Counillon, F., Bertino, L., Tian-Kunze, X., & Kaleschke, L. (2016). Benefits of
525 assimilating thin sea ice thickness from smos into the topaz system. *The Cryosphere*,
526 *10*, 2745–2761. doi: 10.5194/tc-10-2745-2016
- 527 Xiong, C., & Ren, Y. (2023). Arctic sea ice melt pond fraction in 2000–2021 derived by
528 dynamic pixel spectral unmixing of modis images. *ISPRS Journal of Photogrammetry*
529 *and Remote Sensing*, *197*, 181-198. doi: 10.1016/j.isprsjprs.2023.01.023
- 530 Yang, Q., Losa, S. N., Losch, M., Jung, T., & Nerger, L. (2015). The role of atmospheric
531 uncertainty in arctic summer sea ice data assimilation and prediction. *Quarterly*
532 *Journal of the Royal Meteorological Society*, *141*, 2314-2323. doi: 10.1002/qj.2523
- 533 Yang, Q., Losa, S. N., Losch, M., Liu, J., Zhang, Z., Nerger, L., & Yang, H. (2015).
534 Assimilating summer sea-ice concentration into a coupled ice–ocean model using a
535 lseik filter. *Annals of Glaciology*, *56*(69), 38–44. doi: 10.3189/2015AoG69A740
- 536 Yang, Q., Losch, M., Losa, S. N., Jung, T., Nerger, L., & Lavergne, T. (2016). Brief
537 communication: The challenge and benefit of using sea ice concentration satellite
538 data products with uncertainty estimates in summer sea ice data assimilation. *The*
539 *Cryosphere*, *10*, 761-774. doi: 10.5194/tc-10-761-2016
- 540 Zhang, J., & Hibler III, W. D. (1997). On an efficient numerical method for modeling sea ice
541 dynamics. *Journal of Geophysical Research*, *102*, 8691–8702. doi: 10.1029/96JC03744
- 542 Zhang, J., & Rothrock, D. A. (2003). Modeling global sea ice with a thickness and enthalpy
543 distribution model in generalized curvilinear coordinates. *Monthly Weather Review*,
544 *131*, 845–861. doi: 10.1175/1520-0493(2003)131<0845:MGSIWA>2.0.CO;2
- 545 Zhang, Y.-F., Bushuk, M., Winton, M., Hurlin, B., Gregory, W., Landy, J., & Jia, L.
546 (2023). Improvements in september arctic sea ice predictions via assimilation of sum-
547 mer cryosat-2 sea ice thickness observations. *Geophysical Research Letters*, *50*(24),
548 e2023GL105672. doi: 10.1029/2023GL105672